Journal of Hazardous Materials 418 (2021) 125971

Contents lists available at ScienceDirect

Journal of Hazardous Materials

journal homepage: www.elsevier.com/locate/jhazmat

Research Paper

Importance of seasonal sea ice in the western Arctic ocean to the Arctic and global microplastic budgets

Seung-Kyu Kim [a,*,1], Hee-Jee Lee [a,1], Ji-Su Kim [a,1], Sung-Ho Kang [b], Eun-Jin Yang [b], Kyoung-Ho Cho [b], Zhexi Tian [a], Anthony Andrady [c]

[a] Department of Marine Science, College of Natural Sciences, Incheon National University, 119 Academy-ro, Yeonsu-gu, Incheon 22012, Republic of Korea
[b] Division of Ocean Sciences, Korea Polar Research Institute, 26 Songdomirae-ro, Yeonsu-gu, Incheon 21990, Republic of Korea
[c] Department of Chemical and Biomolecular Engineering, North Carolina State University, Raleigh, NC 27695, USA

ARTICLE INFO

Editor: Dr. L. Angela Yu-Chen

Keywords:
Microplastics
Western Arctic ocean
Ice-trapping
Seasonal sea ice
Snow
Melt pond water
Mass budget

ABSTRACT

Arctic sea ice entraps microplastics (MP) from seawater and atmosphere and is recognized as sink and transport vector of MPs. However, ice-trapped fraction in the global MP budget, contribution of atmospheric input, and linkage among Arctic basins remain unclear. To assess them, we investigated the number- and mass-based data separated by size and shape geometry for MPs in sea ice, snow, and melt pond water from the western Arctic Ocean (WAO). A significant dependency of MP data on measured cutoff size and geometry was found. For the same size range and geometry, sea ice MPs in WAO ($(11.4 \pm 9.12) \times 10^3$ N m^{-3} for $\geq$ 100 μm) were within comparable levels with those in other Arctic basins, but showed closer similarity in polymer and shape compositions between WAO and Arctic Central Basin, indicating the strong linkage of the two basins by the Transpolar Drift. Our budgeting shows that a significant amount of plastic particles ($(3.4 \pm 2.6) \times 10^{16}$ N; 280 ± 701 kilotons), which are missed from the global inventory, is trapped in WAO seasonal sea ice, with < 1% snowfall contribution. Our findings highlight that WAO ice zone may play a role as a sink of global MPs as well as a source of Arctic MPs.

1. Introduction

Plastic production has grown over the past 70 years, reaching a cumulative total of 8300 million metric tons to date (Geyer et al., 2017). Reportedly, ~3% of this global production enters the ocean annually, and this amount will double over the next 30 years (Jambeck et al., 2015). In line with this, the abundance of small plastic particles, i.e., microplastics (MPs), in the environmental samples has increased in recent decades (Tekman et al., 2017; Brandon et al., 2019). However, based on a comparison of the values reported in the literature (Cózar et al., 2014; Eriksen et al., 2014; Law et al., 2014; Jambeck et al., 2015; van Sebille et al., 2015; Lebreton et al., 2017), the standing stocks of these small plastic debris afloat in global oceans account for only < 2% (mass base) of the annual plastic input into the ocean and the reasons for this large gap regarding the MP budget remain unsolved.

As a dead end for global surface currents, the Arctic Ocean is suspected of being an unidentified sink that accounts for the "missing" parts of the global MP budget (Cózar et al., 2017). MPs are ubiquitous, and considerable quantities prevail in Arctic compartments, including seawater (Lusher et al., 2015; Kanhai et al., 2018; Mu et al., 2019a), organisms (Kühn et al., 2018; Moore et al., 2020), and seafloor sediments (Tekman et al., 2017; Mu et al., 2019b). Specially, there is growing evidence that Arctic sea ice entraps MPs several orders of magnitude higher than seawater and thus can be a temporary sink and transport vector of MPs in the Arctic Ocean (Obbard et al., 2014; Peeken et al., 2018; Kanhai et al., 2020). Recent studies propose that atmospheric transport and deposition may also contribute significantly to MP abundance in this remote sea ice (Bergmann et al., 2019; Evangeliou et al., 2020). However, little is known about how many parts of the global MP budget are trapped in Arctic sea ice, how much atmospheric input contributes to the ice-trapped MPs, and how the linkage between Arctic basins was reflected in ice-trapped MPs.

This lack of knowledge is related with stark differences in the cutoff size and geometry applied for MP analysis among Arctic studies, undermining a reliable budgeting for Arctic MP source and sink estimates. Compared with seawater samples (mostly ≥ 330 μm including all

* Corresponding author.
E-mail address: skkim@inu.ac.kr (S.-K. Kim).
[1] These authors contributed equally to this work.

https://doi.org/10.1016/j.jhazmat.2021.125971
Received 4 February 2021; Received in revised form 21 April 2021; Accepted 22 April 2021
Available online 8 May 2021

MP geometries) (Lusher et al., 2015; Cózar et al., 2017; Kanhai et al., 2018; Mu et al., 2019a), sea ice and snow were analyzed for ≥ 11 μm nonfiber MPs (Peeken et al., 2018; Bergmann et al., 2019) or all MP geometries ≥ 100 μm (Kanhai et al., 2020). All of the Arctic MP studies have reported MP data as particle number per volume (i.e., N m^{-3}), which is alterable depending on the measured MP cutoff size (Kooi and Koelmans, 2019; Lee et al., 2021) and MP fragmentation degrees (Song et al., 2017). Consequently, there are large gaps in number-based MP loads between ice-free Arctic seawater (~10^{11} N) (Cózar et al., 2017) and yearly melt sea ice (~10^{20} N) (Peeken et al., 2018), and in sea ice MP composition among studies (Peeken et al., 2018; Kanhai et al., 2020). Thus, fragmentation-independent MP data (mass per volume) and harmonization of analyzed MP size ranges and geometries are needed to enable reliable flux and total MP load calculation.

The western Arctic Ocean (WAO) at the Amerasia Basin (AB) includes the East Siberian Sea, Chukchi Sea, and Beaufort Sea. The WAO is geographically connected to the North Pacific Ocean, which contains higher MPs than other oceans (van Sebille et al., 2015; Isobe et al., 2019), and the area where the Transpolar Drift Stream, which may be responsible for transporting WAO MPs into the Arctic Central Basin (ACB) and the Eurasia Basin (EB), begins (Renner et al., 2014). The WAO not only represents the largest summer sea ice losses in the Arctic Ocean (Stroeve and Notz, 2017), but also experiences a rapid transition in sea ice, including a significant reduction in the sea ice extent, the replacement of thick multiyear ice with thin first-year ice, and an increase in the total areal coverage of melt ponds in summer (Nicolaus et al., 2012; Stroeve and Notz, 2017). Considering sea ice's role as a temporal sink and transport vector for MPs (Peeken et al., 2018; Kanhai et al., 2020), the ice-associated MP load and budget in the WAO are important for budgeting MP source and sink estimates in the entire Arctic and worldwide. Compared with the EB and ACB, however this region remains largely unexplored to date.

Here, we analyzed the MP content and composition in ice cores, snow, and melt pond water (MPW) on the WAO sea ice floes to assess whether this region is a global sink and a source in the Arctic, as well as whether atmospheric deposition is a significant input pathway to ice-trapped MPs of this region. To budget MP load, MP mass per volume was estimated from the observed size and geometric shape of individual polymer particles. The effects of measured MP types (cutoff size range and geometry (nonfiber and fiber)) on concentration, budget, size

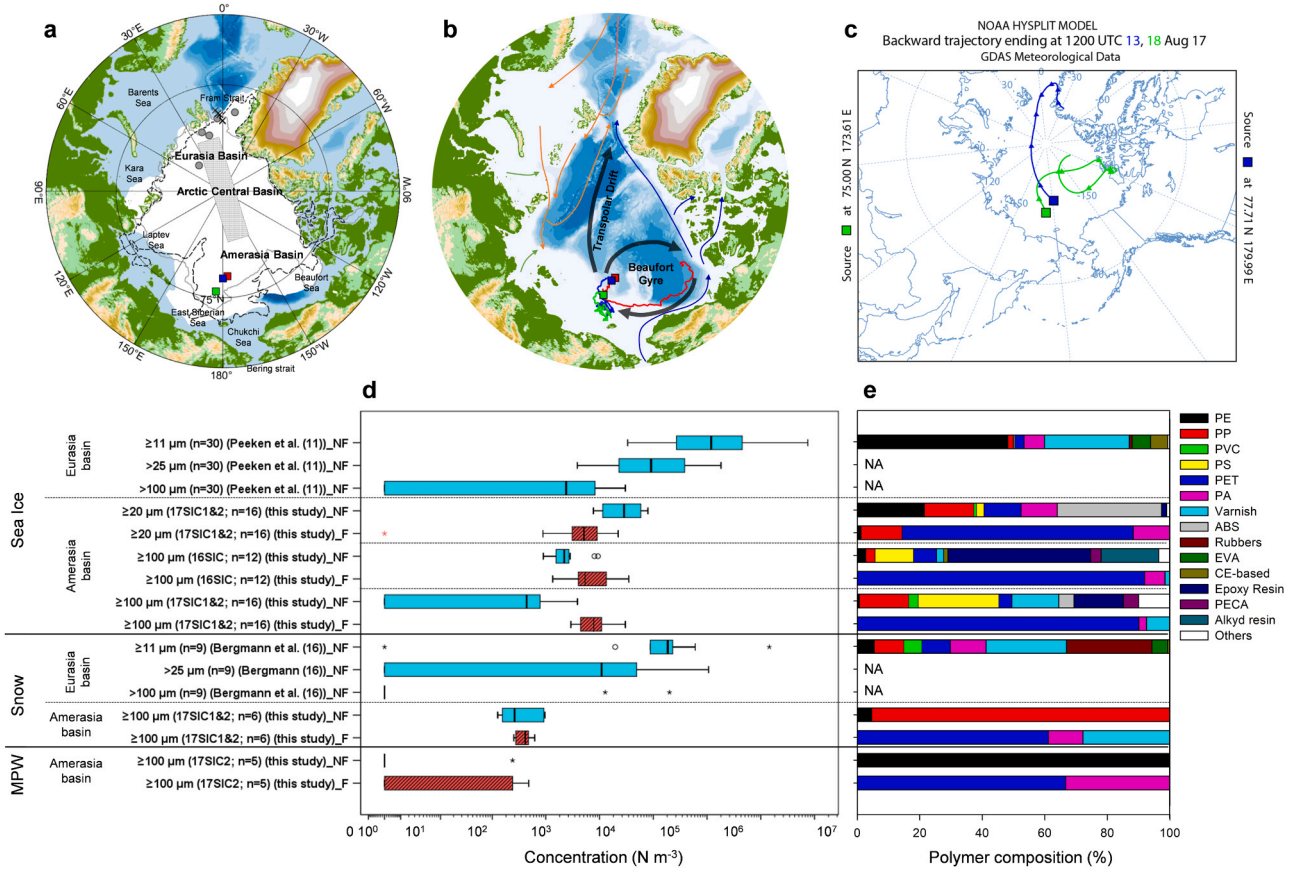

Fig. 1. Potential pathways and pollution characteristics of MPs in the Arctic basins. (a) Locations of ice floes sampled in this study (red square for 16SIC, blue square for 17SIC1, and green square for 17SIC2) and in previous studies (gray circles for sea ice (Peeken et al., 2018) and X for ice floe snow (Bergmann et al., 2019) in the EB, and the dotted area for sea ice in the ACB (Kanhai et al., 2020)). Retreat lines of the sea ice extent are presented for the last 10-year September mean (white-covered area (ASIMS, 2020)) and for the sampling dates in 2016 (dotted line; NSIDC data based on Nolin et al. (1998)) and 2017 (gray-line; NSIDC data based on Brodzik and Stewart (2016)). (b) Drift trajectories of sea ice floes (red line for 16SIC, blue line for 17SIC1, and green line for 17SIC2) and a schematic view of Arctic surface water flows (blue arrows for Pacific water, orange arrows for Atlantic water, and green arrows for terrestrial water). The bold-black arrows indicate the Beaufort Gyre and Transpolar Drift Stream. (c) Seven-day air mass backward trajectories from the NOAA HYSPLIT model. In (d) and (e), the size-segregated concentration range (d) and average polymer compositions (e) of nonfiber ("NF") and fiber ("F") MPs found in the Arctic compartments are compared. In (d), the upper and lower boundaries of the box indicate the 75th and 25th percentiles, respectively. The line within the box marks the median, and the whiskers indicate the minimum and maximum values with the exceptions of outliers (circles) and extremes (asterisk). In (e), PE-based polymers (PE-chlorinated, PE-oxidized, and PE) were summed to PE, acrylic/PUR/varnish/lacquer to varnish, all rubber types to rubbers, and cellulose (CE)-based polymers (CE acetate, CE chemical modified, or CE nitrate) to CE-based. The category of 'others' includes minor polymers (PE-PP, PVA, POM, rosin ester, polycarbonate, polycaprolactone, polylactic acid, and polyimide). Polyester (PES) and nylon were treated with PET and PA, respectively. "NA" stands for not available because the literature does not provide size-segregated polymer compositions.

distribution and polymer composition were investigated for number- and mass-based data. These data were also compared with previous Arctic sea ice (Peeken et al., 2018; Kanhai et al., 2020) and snow (Bergmann et al., 2019) MP data to evaluate any MP linkages or discrepancies among the Arctic basins connected along the Transpolar Drift. To our best knowledge, this study presents the first mass budget of plastic particles in Arctic environment.

2. Materials and methods

2.1. Sampling

In August 2016 and 2017, three sea ice floes drifting in the northern part of the Chukchi Sea were visited during the Korean *IBRV Araon* expeditions: one ice floe during the 2016 expedition (16SIC: 77° 59.65′ N, 178° 58.18′ W) and two ice floes during the 2017 expedition (17SIC1: 77° 42.60′ N, 179° 59.84′ E and 2017SIC2: 75° 33.90′ N, 196° 05.60′ E) (Fig. 1a and Table S1). Seven ice cores were collected from the 16SIC ice floe, and ten ice cores each were collected from the 17SIC1 and 17SIC2 ice floes. The cores were drilled using a Mark II ice corer (9 cm diameter; Kovacs Enterprise; Roseburg, USA). The ice core samples were immediately wrapped in precleaned aluminum foil, transferred into polyethylene bags, and stored at − 20 ℃ prior to pretreatment. Snow sampling was conducted during the 2017 expedition. Three snow samples each were collected from the 17SIC1 and 17SIC2 ice floes. To avoid potential contamination from the vessel and/or research activities, the sampling spots were selected in headwind areas more than 100 m away from the research vessel, and no other anthropogenic activities were conducted in this area before the samples were collected. During snow sample collection, all the personnel were careful to remain downwind of each sampling spot. After removing the surface layer of ~1 cm to completely rule out the possibility of artificial inputs, the subsurface snow layer of a few cm in depth (equivalent to ~7 L of melted water) was collected using a precleaned stainless-steel shovel, stored in a precleaned stainless steel bucket with a stainless-steel lid, and then immediately melted on a hot plate (50 ℃) in the laboratory. The MPW was only collected from the 17SIC2 ice floe. No accessible melt ponds were found on the 17SIC1 ice floe. Five melt ponds had salinity values below 1.1 psu (Table S1). For each melt pond, ~4 L of water was directly collected into a glass bottle covered with precleaned aluminum foil from the subsurface (~5 cm below the surface) using silicon tubing connected to a peristaltic pump (JSW600; JenieWell®). Before collecting the samples, the pumping system was washed in running water for more than 30 min.

2.2. Analytical procedure for synthetic polymers

The collected ice cores had a depth range of 83–218 cm (n = 27; 128 ± 34 cm), and the 16SIC cores (n = 7; 150 ± 32 cm) were slightly thicker than the 17SIC1 (n = 10; 105 ± 23 cm) and 17SIC2 (n = 10; 137 ± 32 cm) cores. Sea ice core samples were treated in two ways. First, the entire column (one-layered ice cores (n = 2); 16SCI-ST1 and ST7) of a single core or each separated into two horizontal layers (upper and bottom layers; almost half to half of an entire depth) of a single core (13 cores; five cores of 16SIC, five cores of 17SCI1, and three cores of 17SIC2) was individually melted down as each sample. These one- and two-layered samples (herein, Sea ice-I) were analyzed to determine MP content in a single core and to investigate the difference in MP content between the upper layer that might be initially formed in the surface of source region and the bottom layer that might be formed in subsurface by downward growth during ice floe transport, respectively. For these Sea ice-I samples (a total of 28 layers from 15 cores), MPs ≥ 100 μm in 3.3 ± 1.2 L per sample were analyzed. Secondly, further analysis was conducted for three cores (two cores from ice floe 17SIC1 and one core from ice floe 17SIC2), each of which was horizontally subsectioned into several layers with a 20-cm-thick using a bone saw. A total of 16 layers from three cores (n = 5 for 17SIC1-ST2 with 0–100 cm, n = 5 for 17SIC1-ST8 with 0–101 cm, and n = 6 for 17SIC2-ST5 with 0–122 cm) were obtained for MP analysis and the melted volume of each layer sample was 0.8 ± 0.3 L per sample. MPs ≥ 20 μm in these multi-layered core samples (herein, Sea ice-II) were measured to investigate the presence of localized sources that might be reflected in the vertical variability of MPs within each single core and to validate the presence and distribution of MPs smaller than 100 μm.

Before melting the cores, the fragile snow-pack layer at the surface of each core was removed, and only the solid interior layers of ice were analyzed. To exclude sample contamination, several millimeters of core surface was also removed using a precleaned stainless-steel grater, and the exposed faces were washed with MP-free water as described in Peeken et al. (2018). Each surface-cleaned core sample was melted in a precleaned glass bottle covered with precleaned aluminum foil at 50 °C.

Each of melted Sea ice-I core water sample, melted snow water sample and MPW sample was filtered through a glass fiber filter (Ø = 47 mm; pore size, 2.7 μm; GF/D, Whatman, Germany). For the Sea ice-I, the snow, and the MPW samples, all the suspected MP particles (i.e., MP-like particles) of ≥ 100 μm on the filter were preselected for characterization. After the size and shape of individual MP-like particles were measured under a stereomicroscope (Leica S8APO; 10–80×), their polymer identifies were determined using the attenuated total reflection mode of a Fourier-transform infrared spectroscopy (FTIR; Agilent Cary 630), as described in our previous study (Supplementary material section-I) (Kim et al., 2018). Although the MP-like particles of ≥ 100 μm preferentially analyzed, some of the particles < 100 μm (0.9% of total plastic particles) were included when their polymer identities were clear from the FTIR spectra.

For Sea ice-II samples, after filtering through a stainless-steel sieve (Ø = 47 mm; pore size, 20 μm; thickness, 15 μm), the digestion process using 35% H_2O_2 was additionally performed to remove interfering organic particles. For the MPs in each layer sample, their polymer identities were determined using the transmission mode of a μ-FTIR microscope (LUMOS; Bruker). In brief, the spectra of all the potential particles ≥ 20 μm in each sieve with no preselection were obtained and then the geometric shapes and sizes of the particles identified as synthetic polymers were measured (see details in Supplementary material section-I). Only 0.76% of the 77,926 particles were synthetic polymers. This approach produced satisfactory recoveries for MP particles with a size range of 27–330 μm in our previous study (Lee et al., 2021).

In our data, rayon, which is semisynthetic cellulose-based fiber, was excluded from the counted MPs due to the close similarity of its FTIR spectra with that of natural polymers (e.g., cellulose and cotton) (Comnea-Stancu et al., 2017), whereas other fibrous synthetic polymers were included.

2.3. Quality assurance and control

To rule out the potential contamination, strict control protocols were conducted during the entire procedure for sample treatment and analysis (see Supplementary material section-I). To monitor potential MP contamination, air and procedural blank samples were analyzed along with every batch of samples. Potential airborne contamination was monitored by exposing clean GF/F papers wet with MP-free water to the laboratory air whenever the samples were exposed to the air. For the procedural blanks, the same volume of MP-free water used for each type of sample was processed in the same way as the samples in every batch. No synthetic particles were found in any of the air (n = 28) and procedural blanks (n = 8) for the Sea ice-I, snow, and MPW samples. The blanks only contained 0–5 non-synthetic (i.e., cotton) fibers per blank. In the Sea ice-II batches for MP ≥ 20 μm, all air blanks (n = 3) contained one PET fiber and 1–2 cotton fibers, and the procedural blanks (n = 3) contained one PET fiber in the 1st batch, none of the synthetic polymers in the 2nd batch, and one PET fiber and one PE fragment in the 3rd batch. Considering the number of synthetic particles detected in Sea ice-

II samples (i.e., 12–80 per sample), the potential contamination was negligible. However, the amount of MP in each of the Sea ice-II samples was corrected by subtracting the amount of PET fiber and PE fragment found in the procedural blanks from the same batch to completely rule out the effect of potential contamination.

2.4. Shape geometry, size distribution, and mass calculation

In this study, MP was defined as synthetic particles $\leq$ 5 mm in size, and mesoplastics were defined as those $>$ 5 mm in size based on the lengths of their longest dimension. All the synthetic polymer particles were classified into four shape groups based on their morphological features, i.e., fragments, sheets, spherules, and fibers, as was done in a previous study (Hidalgo-Ruz et al., 2012), to calculate the shape-dependent particle volume (see Supplementary material). The individual particles were further categorized as nonfiber (sum of fragment-, sheet-, and spherule-type polymers) and fiber particles in the data presentation for consistency with other studies (Peeken et al., 2018; Bergmann et al., 2019). For size distribution, the concentrations of the synthetic polymers in each size class obtained based on number and mass were normalized by the width of the size-class interval to render MP concentrations independent of the bin width (Cózar et al., 2014; Cózar et al., 2017) (see Supplementary material section-II). The observed size distributions of nonfiber and fiber particles were compared with those predicted by three-dimensional (3D) and one-dimensional (1D) steady-state fragmentation models, respectively. For the 3D and 1D fragmentation models, a parallelepiped shape for the nonfibers and a cylindrical shape for the fibers were assumed to be the standard geometric shape, since most of the nonfibers were fragment type (92.4% in Sea ice-I, snow, and MPW for the $\geq$ 100 μm plastic particles and 99.8% in Sea ice-II for the $\geq$ 20 μm plastic particles), and the fibers had a very uniform thickness (0.017 $\pm$ 0.007 mm; n = 507) throughout its entire length.

In this study, we estimated the masses of the individual MP particles by modifying a method presented in elsewhere (Kim et al., 2018), which is based on the particles' morphological features and original densities:

$$M_{total} = \frac{m_{total}}{V} \quad (1)$$

$$m_{total} = \sum_{j=1}^{n} m_j = \sum_{j=1}^{n} (\rho_j \times v_j) \quad (2)$$

where M_{total} is the total mass-based concentration of the plastic particles (mg m^{-3}) in a sample; V is the sample volume (m^{-3}); m_{total} is the total mass of all of the plastic particles in the sample (mg); m_j is the mass of an individual plastic particle j (mg); $\rho_j$is the original density proposed in literature (Table S2) for the polymer j identified using FTIR (g cm^{-3}); v_j is the estimated volume of the plastic particle j based on its morphological features (mm^{-3}). We measured the length of the largest cross-section and defined it as the length (L_j; mm) of the individual plastic particle j. For the fibrous plastics with a regular shape (i.e., a cylinder-type), we measured both the length and the diameter (or thickness) (d_j; mm) of the individual fiber particle. The volume of the individual particle (v_j) was estimated by classifying its shape as one of the four types according to its morphological features (Supplementary material section-III). The values converted to the mass per volume were used to compare with the number-based concentration (i.e., in N m^{-3}) and to calculate mass-based MP flux and load.

2.5. MP budgeting for Arctic load

The amounts of plastic particles trapped in (or released from) sea ice and deposited via snowfall scavenging were calculated for the area of the WAO (150°E (East Siberian Sea) to 120°W (Beaufort Sea); 66°34′N (Bering Strait) to the 10-year mean September retreat line), which repeats the formation and melting of sea ice yearly. The last 10 years (2008–2017) of mean sea ice coverage data (ASIMS, 2020) indicate that approximately 1.9 $\times$ 10^6 km^2 (equivalent to a volume of 2.9 $\times$ 10^3 km^3 assuming an average 1.5 m ice thickness (Petty et al., 2016)) of sea ice is formed and melted annually in the assigned study domain. Based on the annual snowfall (~180 mm $year^{-1}$) in the WAO (Boisvert et al., 2018), the same area is estimated to receive annual snowfall of ~350 km^3. The densities of 910 kg m^{-3} for sea ice (Timco and Frederking, 1996) and 300 kg m^{-3} for snow (Warren et al. 1999) were used to estimate their water-based volumes, and the densities of the melted sea ice and snow samples were assumed as water density (1000 kg m^{-3}).

2.6. Data comparison and reanalysis

The WAO data (this study) were compared with those from the other Arctic basins on the Transpolar Drift path. Data on MP in sea ice (Peeken et al., 2018) and snow (Bergmann et al., 2019) from the EB were fully available without restriction at the open database in the PANGEA public repository (http://doi.pangaea.de/10.1594/PANGEA.886593 for sea ice and http://doi.pangaea.de/10.1594/PANGEA.901447 for snow), which provides the number-based concentrations for total MP particles with size classes (a bin width of 25 μm) and for polymers without size classification. Their data were reanalyzed to obtain normalized size distribution, size-segregated concentration ($\geq$ 11 μm, $\geq$ 25 μm, and $\geq$ 100 μm), and average polymer composition. Data comparison was available only for nonfiber MPs, since the polymer identities of the fiber particles were not determined for the Eurasian samples. Data for snow fiber particles presented in Bergmann et al. (2019) were not considered because microfibers in natural samples are mainly composed of natural polymers (Suaria et al., 2020). The comparison with the ACB sea ice was based on the data (number-based total MP concentration) and description (polymer composition in total MPs) presented in the literature (Kanhai et al., 2020).

2.7. Back-trajectories of sea ice floes and air masses

We used the Lagrangian particle tracking method (LPTM) to estimate sea ice trajectories. The LPTM traces the path of sea ice backward in time using a combination of sea ice motion vectors (SIMV) and sea ice concentrations to determine the origin and pathways of the sea ice floes. The SIMV data and daily sea ice concentration data were obtained from the Polar Pathfinder Daily 25 km EASE-Grid data provided by the National Snow & Ice Data Center (NSIDC) (Tschudi et al., 2019) and from the sea ice data archive provided by the University of Bremen (Spreen et al., 2008), respectively. The backward tracking stopped if either the SIMV value was equal to zero or the sea ice concentration was lower than 15% at a specific location for ten consecutive days. We assessed the uncertainties in the estimated sea ice trajectories by comparing them with the pathways of ice buoys provided by the International Arctic Buoy Programme (http://iabp.apl.washington.edu/data.html). We retracked eight ice-buoy tracks available from January to May in 2017 and 2018 around the study area. The average displacement of the backward tracked buoys during the first 30 days was approximately 15 km, and it linearly increased to ~80 km over 150 days of tracking. The origin of the air masses associated with snowfall at the 17SIC1 and 17SIC2 ice floes was modeled with the Hybrid Single-Particle Lagrangian Integrated Trajectory (HYSPLIT) (Draxler and Rolph, 2003), using seven-day backward air mass trajectories at 500 m and 1000 m a.s.l. based on the Global Data Assimilation System meteorological data set.

3. Results

This study presents data for two geometries (nonfiber (a sum of fragment-, sheet-, and sphere-shaped polymers) and fiber) of MPs ($\leq$ 5 mm) and mesoplastics ($>$ 5 mm). Mesoplastics were detected only in Sea ice-I ((1.20 $\pm$ 1.09) $\times$ 10^3 N m^{-3}) and snow ((0.14 $\pm$ 0.18) $\times$ 10^3 N m^{-3}) samples, all of which were fiber-type. Subsequent analyses and

discussion of the data, except for the size distribution and mass budget, were conducted for MPs ≤ 5 mm.

3.1. Sea ice-I, snow, and MPW (MPs ≥ 100 μm)

For consistency, we first compared number-based data for MP ≥ 100 μm in Sea ice-I, snow, and MPW samples obtained from three WAO sea ice floes during the 2016 and 2017 summers. The concentrations of total MPs (a sum of nonfiber and fiber MPs) in Sea ice-I cores (n = 28) were (11.4 ± 9.12) × 10^3 N m^{-3} with more frequent (detection frequency=100%) and more abundant (84 ± 17% of total MP) fiber types than nonfiber type (detection frequency=79%) (Table 1). No significant differences in fiber MP concentrations were found among the cores of three different ice floes (n = 12 for 16SIC, n = 10 for 17SIC1, and n = 6 for 17SIC2) (Kruskal-Wallis test: p = 0.287). For nonfiber MP concentrations, the 16SIC and 17SIC cores were significantly different (Mann-Whitney *U*-test: p < 0.001), with a 5-fold higher MP concentration in 16SIC cores, but there was no significant difference between the 17SIC1 and 17SIC2 cores (Mann-Whitney *U*-test: p = 0.22). The estimated tracks of the sampled sea ice floes showed different drift trajectories and source regions (Fig. 1b). Ice floe 16SIC traveled a longer distance, following the Beaufort Gyre after forming in the Beaufort Sea, while those of 17SIC1 and 17SIC2 originated in the East Siberian Sea. Our result implies that more nonfiber MP particles originating from the Beaufort Sea were incorporated into the ice cores than those from the East Siberian Sea.

MPs were detected in all ice floe snow samples, but the total MP concentration ((0.87 ± 0.36) × 10^3 N m^{-3}) was an order of magnitude lower than those in the Sea ice-I cores from the same ice floes. Different from ice cores containing 15-fold more fiber types than nonfiber types, the snow samples exhibited similar concentrations for the two geometries (Mann-Whitney *U*-test: p = 0.69), with fiber MPs accounting for 54 ± 24% of the total MP. Thus, the MP origins for sea ice and ice floe snow may differ. The air mass back-trajectories show that MPs in snow on ice floes 17SIC1 and 17SIC2 were transported from the northern coasts of Greenland and the Canadian Archipelago, respectively at 1000 m a.s.l. (Fig. 1c), or both moved from Greenland coasts at 500 m a.s.l. (Fig. S1). Neither nonfiber nor fiber MPs had significantly different concentrations between the two ice floe snow samples (Mann-Whitney *U*-test: p > 0.05 for each).

The MPW samples recorded the lowest total MP levels, (0.24 ± 0.29) × 10^3 N m^{-3}, which were significantly lower than those in sea ice (Mann-Whitney *U*-test; p < 0.001) or snow (Mann-Whitney *U*-test; p = 0.017) (Fig. 1d and Table 1). MPs were detected in only three of five MPW samples. Despite the low occurrence of MPs in MPW, their concentrations were several orders of magnitude higher than those in Arctic surface water (Lusher et al., 2015; Kanhai et al., 2018; Mu et al., 2019a) and thus reflected the enhanced MP amount released from sea ice and snow. The predominance of fiber type (89 ± 19% of total MP) in MPW samples indicated potentially more input from sea ice melt than snow melt.

In the present study, a total of 17 different polymer types were identified by FTIR (Table S2): polyethylene (PE), polypropylene (PP), PP-PE copolymer (PP-PE), polyvinyl chloride (PVC), polyurethane (PUR), polystyrene (PS), polyethylene terephthalate (PET), acrylic, polyamide (PA), epoxy resin, acrylonitrile butadiene styrene (ABS), polyvinyl acetate (PVA), polyoxymethylene (POM), poly(ethyl cyanoacrylate) (PECA), cellulose nitrate (CE-nitrate), rosin ester, and alkyd resin. The polymer composition varied according to the geometry, compartment, cutoff size, and source region (Fig. 1d). First, three polymers (PET, PA, and acrylic), which are major fiber plastics produced globally (Geyer et al., 2017), accounted for most of fiber MPs found in Sea ice-I (99.8%), snow (100%), and MPW (100%) but were minor components for nonfiber MPs (< 6%). For fibrous MPs, PET fibers were predominant in all compartments (91%, 61%, and 67%, respectively). On the other hand, other polymers (epoxy resin, alkyd resin, PS, and PP) were more prevalent in nonfiber MPs. This indicates that polymer composition of total MPs may vary depending on the relative proportions of the two geometries. Second, PA and acrylic fibers comprised 4.8% and 4.2% of fiber MPs in Sea ice-I, while their proportions increased to 11% and 28%, respectively, in snow samples; acrylic fibers were not found in MPW. Inter-compartment discrepancies was much obvious for nonfiber MPs. Epoxy resin, PS, and alkyd resin were the most abundant (each > 10% of nonfiber MPs) in Sea ice-I, while PP (90%) and PE (10%) in snow and only PE in MPW were detected as nonfiber MPs. Third, despite the similarity in fiber MPs, major polymers that made up nonfibers differed between ice floes with different origins. Epoxy resin (46%), alkyd resin (18%), and PS (12%) were highly abundant nonfiber MPs in the 16SIC cores, while PS (26%), epoxy resin (16%), and PP (16%) were more abundant in the 17SIC1 and 17SIC2 cores than other nonfibrous polymers (each < 5%). Alkyd resin was not found in the 17SIC cores. PE was rarely found in all Sea ice-I samples and accounted for only 2% of nonfiber MPs.

The polymer composition of total MPs demonstrated the different MP origins by compartment and source region in a principal component analysis (PCA) plot (Fig. 2). The 17SIC ice core samples originating from the same source region (the East Siberian Sea) constituted cluster-I despite their layers (upper and bottom) and locations (17SIC1 and 17SIC2), reflecting the PET predominance (mean 84% of total MPs). The 16SIC ice core samples originating from the Beaufort Sea (cluster-II) overlapped or separated from cluster-I according to relative proportions of PET (mean 68%) and other polymers (epoxy resin, alkyd resin, and PS). Most of the snow samples (cluster-III) were completely separated from sea ice samples by a relatively low PET proportion (mean 34%) and more abundant PP (mean 43%) compared with those of the 16SIC (PP 1.3%) and 17SIC (PP 0.8%) sea ice samples. MPW samples were not included in the PCA since only PET, PA, and PE were detected, but they were much closer to the ice core samples due to PET dominance (56%).

3.2. Sea ice-II (MPs ≥ 20 μm)

MP totals of ≥ 20 μm quantified in the vertical multilayers of Sea ice-

Table 1
Comparison of the number-based and mass-based concentrations of synthetic polymers in the WAO samples collected in this study.

Sample type	Minimum size of MPs	Number of sample	Number-based concentration (×10^3 N m^{-3})			Mass-based concentration (mg m^{-3})		
			nonfiber	fiber	total plastics	nonfiber	fiber	total plastics
MPs (≤5 mm)								
Sea ice-I	≥ 100 μm	n = 28	1.67 ± 2.24	9.77 ± 8.36	11.4 ± 9.12	99.8 ± 264	3.69 ± 3.13	103 ± 264
Sea ice-II	≥ 20 μm	n = 16	36.0 ± 26.8	7.21 ± 6.60	43.2 ± 32.0	3.06 ± 3.47	2.00 ± 1.41	5.05 ± 4.75
Snow	≥ 100 μm	n = 6	0.46 ± 0.39	0.41 ± 0.14	0.87 ± 0.36	17.8 ± 16.5	0.75 ± 0.38	18.5 ± 16.2
MPW	≥ 100 μm	n = 5	0.05 ± 0.11	0.19 ± 0.20	0.24 ± 0.29	1.95 ± 4.36	0.14 ± 0.15	2.09 ± 4.48
Mesoplastics (> 5 mm)								
Sea ice-I	≥ 100 μm	n = 28	0	1.20 ± 1.09	1.20 ± 1.09	0	1.90 ± 1.62	1.90 ± 1.62
Sea ice-II	≥ 20 μm	n = 16	0	0	0	0	0	0
Snow	≥ 100 μm	n = 6	0	0.14 ± 0.18	0.14 ± 0.18	0	1.27 ± 2.08	1.27 ± 2.08
MPW	≥ 100 μm	n = 5	0	0	0	0	0	0

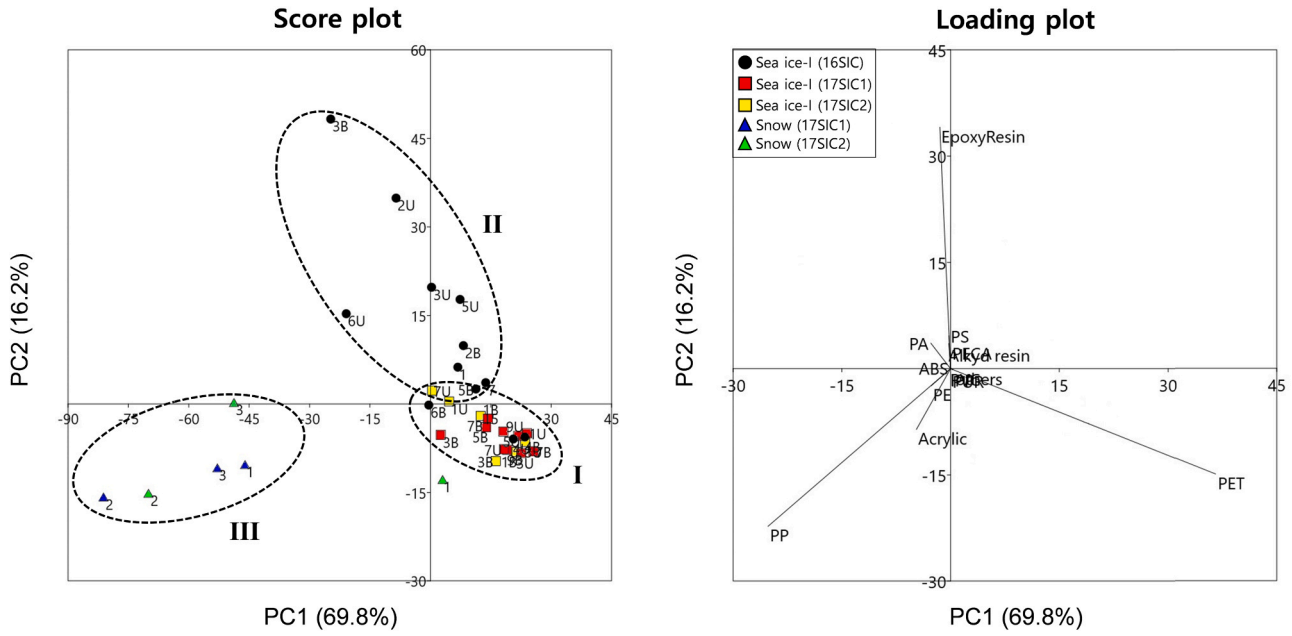

Fig. 2. PCA loading and score plots of MP (≥ 100 μm in size) in Sea ice-I core and snow samples. The relative proportions of individual polymers to total MP with no separation of its geometry were used as an input variable. The capital letters U and B on the score plot indicate the upper and bottom layers of the Sea ice-I core, respectively. Minor polymers (PVA, POM, CE-nitrate, and rosin ester) were grouped together as "others".

II samples (total n = 16) collected at 17SIC1 and 17SIC2 produced completely different results collected from the same ice floes from those in Sea ice-I in terms of both concentration and composition (Fig. 1d and e). Nonfiber MPs, which were rare in Sea ice-I, showed ~60 times higher number-based concentrations in Sea ice-II than in Sea ice-I (Table 1). Fiber MPs, which were mostly present as large particles in both Sea ice-I and II (see "later section for size distribution"), did not exhibit a significant concentration difference between Sea ice-I and Sea ice-II (Mann-Whitney *U*-test: p = 0.149). Sea ice-II contained a 4 times higher total MP concentration and a greater nonfiber contribution to the total MP (82 ± 11%) than Sea ice-I, which was dominated by fibers. The most abundant nonfiber polymer types in Sea ice-II were ABS (33% of nonfiber MP), followed by PE (22%), PP (16%), PET (12%), and PA (11%). Though rare in Sea ice-I samples, PE was abundant in Sea ice-II samples. This shows that the nonfiber type of this commercially important polymer is mostly present as smaller particles (< 100 μm) in Arctic sea ice. For fiber types, PET was still dominant (74% of fiber MPs) in Sea ice-II samples, followed by PP (13%) and PA (12%). Our results show that the concentration and polymer composition of total MPs can be significantly altered depending on the analyzed cutoff size because nonfiber types are more prevalent in the small-size classes (< 100 μm) than fiber types.

3.3. Vertical MP profiles in sea ice cores

MPs found in Sea ice-I cores did not show drastic differences between top and bottom layers in any cores (Figs. S2 and S3). The total MP concentration difference in the two layers of a single core was within a factor of three, and their polymer compositions were similar, with PET predominance. Likewise, the multilayers of Sea ice-II cores had vertically uniform MP distributions. MP concentrations were 2- to 10-fold in a single core, with no correlation between subsection depth (or salinity) and MP concentration. The polymer composition, despite one slight difference, was vertically similar, with ABS, PE, and PP for nonfibers and PET for fibers as the major components (Fig. 3). Interestingly, the concentrations of nonfibers and fibers were positively correlated in their vertical distributions (Spearman's $r_s = 0.597$; p = 0.015), indicating that the two geometric types may have the same source (likely the East Siberian Sea water). Our results show the presence of non-localized MPs along the drift path of each ice core or the rapid growth of ice cores, assuming that the downward growth of an ice core incorporates MPs from seawater contacted at different locations.

3.4. Number-based size distribution

In the number-based size distribution, both nonfiber and fibers exhibited Gaussian-type size distributions rather than power-law distributions, and peak concentrations (i.e., modes) appeared in different size classes according to particle geometry and sample type (Figs. 4a and S4). Compared with nonfiber particles, most of the fiber particles (55–100%) in all the samples demonstrated sizes larger than a common mesh size for surface seawater sampling (≥ 330 μm), and > 5 mm fibers were also frequently found (Fig. S5). Thus, fiber particles had modes in size classes larger than those of nonfiber particles. For the Sea ice-I and snow to both of which the same analytical method was applied, smaller particles were richer in Sea ice-I than snow. This finding represents additional evidence of the different origins of plastic particles in these two compartments. The Sea ice-II modes shifted to size classes smaller than those of Sea ice-I, indicating that some small plastic particles were likely missed due to human bias in the particle preselection method used for Sea ice-I. Unlike the WAO samples, the Eurasian sea ice and snow had a power-law distribution (Fig. 4a).

The observed size-normalized concentrations were better predicted by a 3D model for nonfibers but a 1D model for fibers (Fig. 4a). The different size distribution between nonfiber and fiber has been also frequently found in previous studies for agricultural soils (Kim et al., 2021) and table salts (Lee et al., 2021; Kim and Song, 2021). They commonly demonstrated more abundant fibers in large size classes and the better prediction by 1D fragmentation model for fiber, compared with those for nonfiber. Song et al. (2017) observed the generation of nonfiber particles (PP, PE, and PS spherules) close to those predicted by 3D steady state fragmentation model (i.e., a power-law distribution with an exponent of ~3) after ultraviolet (UV) exposure coupled with mechanical abrasion. Most of synthetic fiber particles found in the present study consisted of PET, which had a relatively uniform thickness (a median = 15.0 μm; n = 428) regardless of different sizes

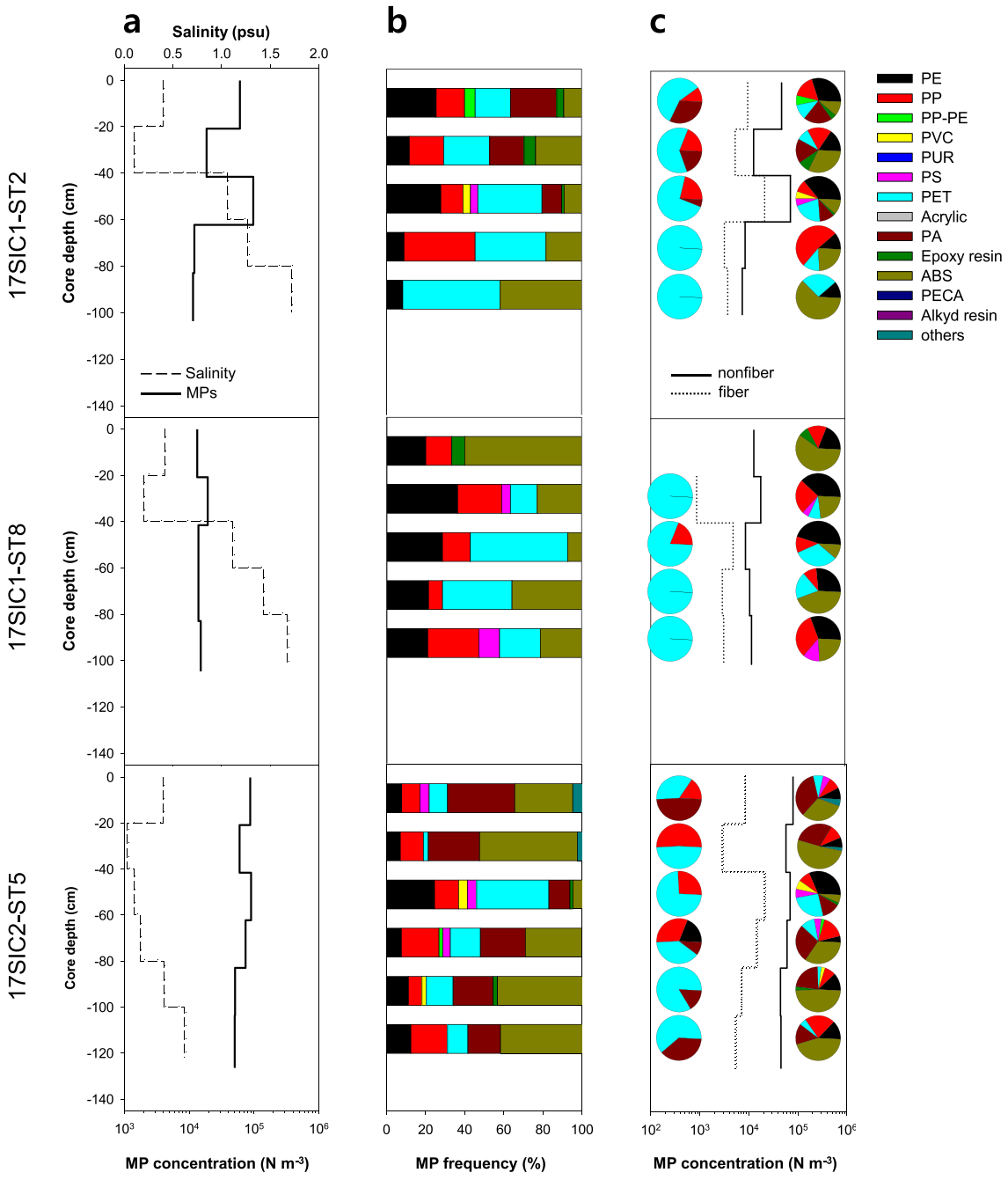

Fig. 3. Vertical MP profiles of Sea ice-II cores. (a) concentration of total MP and salinity. (b) Polymer compositions of total MP and (c) Concentration of nonfiber (solid line) and fiber MP (dotted line) and polymer composition of nonfiber MP (pie charts on the right) and fiber MP (pie charts on the left).

(0.12–16.8 mm) and were similar with a median thickness (15.8 μm) of microfibers collected in oceanic waters (Suaria et al., 2020). Sørensen et al. (2021) found a significant change in PET fiber length from 3115 μm before exposure to 257 μm after 56-day UV exposure in seawater, with no significant alteration in its thickness. Therefore, fiber particles may undergo a different fragmentation mechanism from nonfibers that are three-dimensionally fragmented. Our result suggests that fibers with a cylindrical shape may be mostly fragmented in a way that decreases its length.

3.5. Mass-based concentration and size distribution

To obtain the total MP load independent of the fragmentation degree, we estimated the MP mass per volume for each sample. The estimated MP mass concentrations were 103 ± 267 mg m^{-3} in Sea ice-I, 5.05 ± 4.75 mg m^{-3} in Sea ice-II, 18.5 ± 16.2 mg m^{-3} in snow, and 2.09 ± 4.48 mg m^{-3} in MPW. Mesoplastic mass concentrations were 1.90 ± 1.62 mg m^{-3} in Sea ice-I and 1.27 ± 2.08 mg m^{-3} in snow.

Unlike number-based values, mass concentrations of particularly nonfibers tended to increase as particle size increased (Figs. 4b and S6). In Sea ice-I, the > 330 μm nonfiber MPs comprised 36% of the total number but 97% of the total mass of nonfiber MP particles, and fiber-type mesoplastics accounted for 17% of the total number but 45% of the total mass of fibrous plastic particles. These large-sized plastic particles were absent from Sea ice-II. Consequently, Sea ice-II had a 4-fold higher number-based concentration but a 20-fold lower mass-based concentration than Sea ice-I (Table 1). Therefore, large particles, though less abundant in numbers, contribute more significantly to total

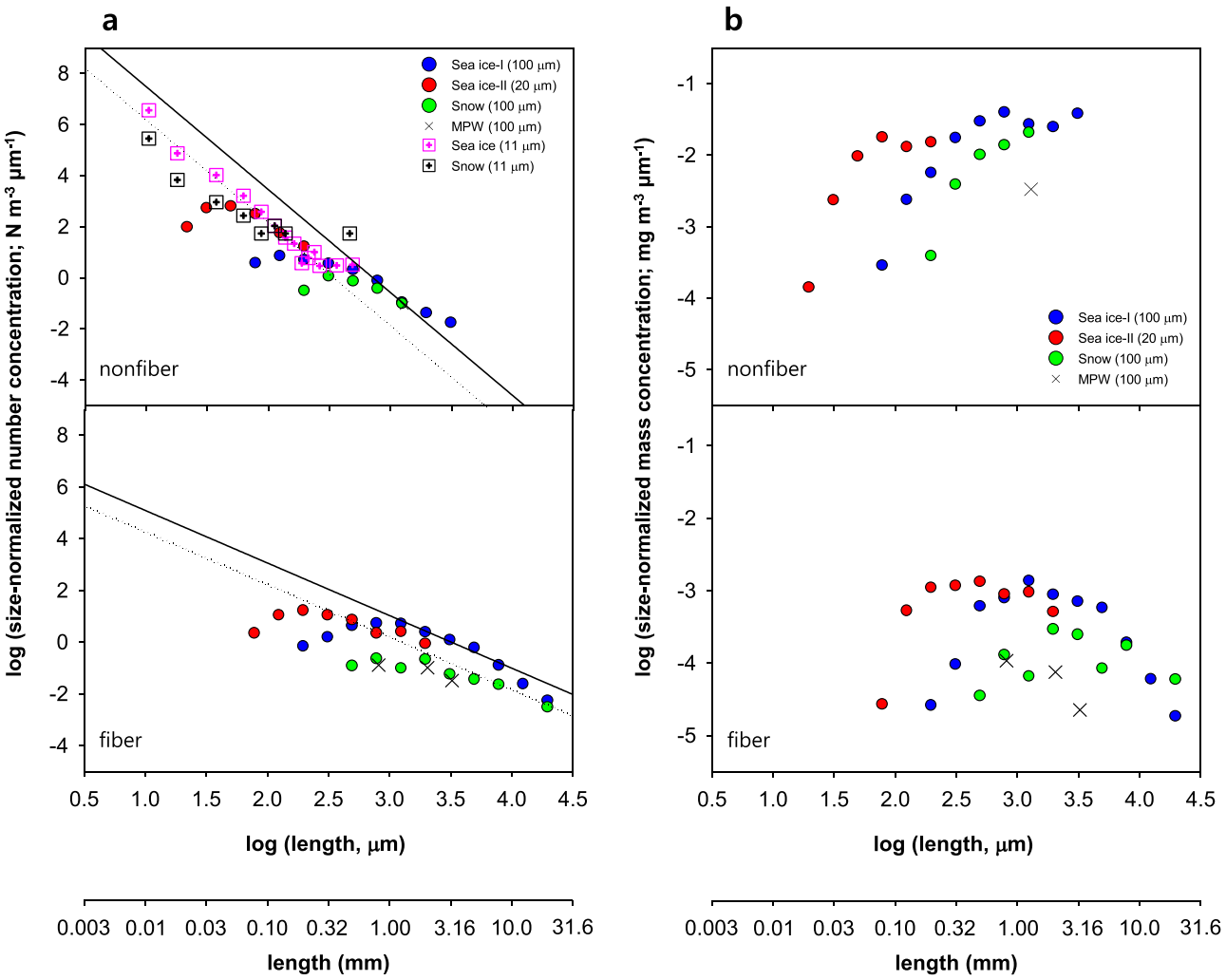

Fig. 4. Size distributions of MP concentration normalized by size. (a) Number-based size distribution and (b) mass-based size distribution. In (a), the observed size distributions in this study (circle- and X-symbols) and in the Eurasian samples (dotted squares for sea ice (Peeken et al., 2018) and snow (Bergmann et al., 2019)) are compared with those expected (solid and dotted lines) from the 3D (nonfiber) and 1D (fiber) steady-state fragmentation models. The solid and dotted lines were calculated using the C_{ref} values from Sea ice-I and -II obtained in this study, respectively (see Supplementary material). The values in legend parentheses indicate the minimum MP cutoff size. For this size distribution, all the polymer particles, including > 5 mm, were considered.

mass load. For geometry, MP number concentrations were mostly composed of fiber (84% in Sea ice-I, 54% in snow, and 89% in MPW), while their mass concentrations were dominated by nonfiber (65%, 85%, and 32%, respectively). This dissimilarity relates to the particle volumetric differences between the two geometries, which are proportional to the first and third order of the measured length for fiber and nonfiber, respectively (see Supplementary material section-III). Notably, the mass difference between single nonfiber and fiber particles can be amplified as particle size increase (Fig. S7). It should be noted that large particles (≥ 330 μm or > 5 mm) were found mostly in Sea ice-I, snow, and MPW samples where relatively large volume was used for MP analysis (3.3 ± 1.2 L per sample, 7.1 ± 0.6 L per sample, and 4 L per sample, respectively), compared with Sea ice-II (0.8 ± 0.3 L per sample) and Eurasian samples (sea ice with 1.3 ± 0.3 L per sample (Peeken et al., 2018); snow with 0.08 ± 0.07 L per sample (Bergmann et al., 2019)). Our results indicate that missing large-sized particles, particularly nonfibers, even with little impact on number-based data, can lead to a serious underestimation in the mass load of plastic particles.

3.6. Plastic loads in WAO

Based on the seasonal WAO sea ice coverage data (ASIMS, 2020) and plastic particle concentrations (sum of MP and mesoplastics) obtained in this study, it is estimated that (0.78–11; 3.4 ± 2.6) × 10^{16} N (based on Sea ice-I) to (0.31–2.6; 1.1 ± 0.008) × 10^{17} N (based on Sea ice-II) of plastic particles may be entrapped in sea ice or potentially released into surrounding seawater annually. These amounts correspond to mass loads of 1.1–41 (13.4 ± 12.6) kilotons (Sea ice-II) and 1.7–3600 (280 ± 701) kilotons (Sea ice-I). The mean-based mass loads are comparable to previous estimates of MP stocks afloat in the global oceans and comprise 0.1–2% of the maximum estimate of plastics entering the oceans annually (Table 2). Snowfall deposits (0.67–1.4; 1.1 ± 0.003) × 10^{14} N or 0.26–5.0 (2.1 ± 1.7) kilotons of plastic particles in the same study domain area annually. Snowfall scavenging explains only 0.3% of the mean number load and 0.7% of the mean mass load of the plastic particles trapped in the seasonal sea ice, indicating the nonsignificant atmospheric fall-out contribution.

3.7. Inter-basin relationship

For comparison with other Arctic basins, the number-based data of nonfiber MPs from Eurasian sea ice (Peeken et al., 2018) and ice floe snow (Bergmann et al., 2019), and total MP (sum of all geometries) from the ACB sea ice (Kanhai et al., 2020) were used because of the different

Table 2
Comparison of the annual loads of plastic particles in the WAO study domain area with the estimates for the standing stock of plastic particles afloat in oceanic waters and the annual plastic input into global oceans. The mass load for the MPW was not calculated due to a lack of available data for estimating the MPW volume.

Compartment	Region	Plastic size	Mass load (kilotons)	References
Sea ice trapping	Pacific sector of Arctic Ocean (66°34′N to 10-yr annual sea ice retreat line; 150°E to 120°W)	≥ 100 μm	280 (70)[a]	This study
Snowfall deposition	Pacific sector of Arctic Ocean (66°34′N to 10-yr annual sea ice retreat line; 150°E to 120°W)	≥ 100 μm	2.1 (1.8)	This study
Standing stock in surface seawater	Eastern Pacific Ocean (17.4°S to 61.0°N; 85.0–180.0°W)	≥ 330 μm	21.3[b]	Law et al. (2014)
	North/South Pacific Ocean, North/South Atlantic Ocean, Indian Ocean	≥ 200 μm	6.6—35.2	Cózar et al. (2014)
	North/South Pacific Ocean, North/South Atlantic Ocean, Indian Ocean, Mediterranean Sea	≥ 330 μm	270[b,c]	Eriksen et al. (2014)
	Global ocean standing stock	≥ 150 μm[d]	93—236[c]	van Sebille et al. (2015)
Annual ocean input	Global riverine input		1150—2410	Lebreton et al. (2017)
	Input from 192 coastal countries		4800—12700	Jambeck et al. (2015)

[a] Values from this study indicate the estimates based on mean (median) concentrations found in Sea ice-I and snow samples.

[b] Minimum estimates presented in each literature.

[c] Values estimated by ocean models.

[d] > 90% of quoted data used the mesh sizes of 333 μm and 335 μm.

MP geometries measured among studies. When comparing without distinguishing the minimum cutoff size, the nonfiber MP concentrations of ≥ 100 μm recorded in WAO Sea ice-I and snow were three to four orders of magnitude lower than those of ≥ 11 μm in the Eurasian samples (Peeken et al., 2018; Bergmann et al., 2019). Most nonfiber MPs in the Eurasian samples (99.8% in sea ice and 98.5% in snow) were present below 100 μm, which was the minimum cutoff size for our Sea ice-I and snow samples. When only nonfibers of ≥ 100 μm were compared, Eurasian sea ice ($(4.9 \pm 7.2) \times 10^3$ N m^{-3}) and snow ($(24 \pm 66) \times 10^3$ N m^{-3}; MP ≥ 100 μm were detected in only two of nine snow samples) did not exhibit significant concentration differences from the WAO samples (Mann-Whitney *U*-test: $p = 0.384$ for sea ice and $p = 0.088$ for snow) (Fig. 1d). More recently, Kanhai et al. (2020) reported total MPs ≥ 100 μm in sea ice cores from the ACB, which were estimated to originate from the East Siberian Sea, Chukchi Sea, Laptev Sea, and Central Arctic Ocean. Their total MP concentrations ($(6.5 \pm 3.4) \times 10^3$ N m^{-3}; $n = 25$) were comparable with our Sea ice-I samples, but a concentration difference between the two basins, with a ~2 times higher level in the WAO samples, was significant (Mann-Whitney *U*-test: $p = 0.023$). Compared with Sea ice-II for ≥ 20 μm, Eurasian sea ice (> 25 μm) showed a significantly higher mean concentration (Mann-Whitney *U*-test: $p = 0.014$) but a median concentration within the same order of magnitude (9.35×10^4 N m^{-3} for the EB (Peeken et al., 2018) versus 3.14×10^4 N m^{-3} for the WAO).

The Eurasian data provide polymer compositions in the full size range of ≥ 11 μm, where prevalent varnish was common for both sea ice (27%) and snow (26%), but the dominance of different polymers (PE 48% and rubber < 1% in sea ice versus PE 6% and rubber 27% in snow) distinguished the two compartments (Peeken et al., 2018; Bergmann et al., 2019). Nonfibrous PUR and acrylic, which were assigned to the varnish type in Eurasian samples, were rarely found in Sea ice-I (4 of $n = 28$) or not found in Sea ice-II, snow and MPW samples of the WAO. Sea ice polymer composition differed significantly between the EB and WAO (Fig. S8). A geographical difference in MPs may exist in sea ice source regions (i.e., Laptev Sea, Nansen Basin, and Makarov Basin for Eurasian samples (Peeken et al., 2018) versus East Siberian Sea for WAO samples). However, care is necessary since 67% of nonfiber MPs in Eurasian sea ice were within the smallest detectable size class of 11 μm, considering size-dependent polymer composition found in our study. The ACB ice cores, where the same MP types as those in our Sea ice-I samples (targeting ≥ 100 μm in size and including fiber MP) were analyzed, exhibited the dominance of polyester (probably PET; 57% of total MPs) in polymer type and fiber (79% of total MPs) in geometry (Kanhai et al., 2020). PE in that study accounted for < 1% of the total MPs. Their findings were consistent with those in the WAO Sea ice-I cores, supporting the similar origin of entrapped MPs in sea ice from both basins.

4. Discussion

4.1. Uncertainty in mass estimate

Since we could not weigh individual MP particles, we estimated the masses based on their morphological features. Poulain et al. (2019) also proposed geometry-dependent models (sphere and ellipsoid) to estimate the masses of individual nonfiber MP particles (25 μm to 5 mm). They predicted the masses of ~10 times the difference for the two model geometries and validated that the measured masses of most of the particles fell within the two model estimates. In contrast to their models that need both the measured length and width of a particle, our method for nonfiber particles was based on the measured length alone since it was practically difficult to define the width and/or height of the particle with an irregular shape. Our nonfiber mass estimates fell within those estimated by the two models, close to that of the sphere model but ~10 times higher than that of the ellipsoid model (Fig. S6). Considering the ~10 times higher mass estimates of nonfiber MPs than that predicted by the ellipsoid model, the ice-trapped and snow-deposited mean mass load of plastics presented in our study can be lowered to 6 kilotons (Sea ice-II base) to 41 kilotons (Sea ice-I base) and 0.4 kilotons, respectively. However, they are still substantial in the global MP budget.

Evangeliou et al. (2020) estimated that 5–20% of the total road traffic-originated plastic mass (sum of tire and brake wear particles) emitted globally could reach the Arctic via the atmosphere. In that study, the modeled concentration of road plastics (including PM2.5 and PM10 sizes) in the Arctic snow ranged from 9 to 190 ng kg^{-1}. These concentrations are almost three orders of magnitude lower than our estimates for total plastic particles (sum of MPs and mesoplastics; 2.51–47.7 μg kg^{-1}) in the WAO snow, which is not surprising considering the lower usage of road plastics and different size ranges. For comparison, note that PET of 5.6–23 μg kg^{-1} in Alpine snow (Materić et al., 2020), which was quantified using thermal desorption-proton transfer reaction-mass spectrometry, was ~10 times higher, probably due to the closer proximity to source regions than those of fiber MP

(mostly PET) in the WAO snow (0.55–5.8 μg kg^{-1}). Despite uncertainty originating from the method, comparison with other data shows that our estimates for mass concentration and load are overall within reasonable range. In future studies, polymer-specific mass measurement (Fisher and Scholz-Böttcher, 2017) need to be considered to validate the estimated MP load and budget.

4.2. Potential sources of MPs in the WAO

Our data analysis shows that all the Arctic Ocean basins are polluted with similar MP levels within an order of magnitude, when comparing the same size range and geometry. Specially, the similarity between the ACB and the WAO found in both MP concentration and composition shows that sea ice MPs of the two basins are strongly linked by the Transpolar Drift Stream. Therefore, MPs in the WAO may be largely responsible for the amounts of MP found in other Arctic Basins. MPs in the WAO may originate from various sources, including inflowing seawater, atmospheric deposition, untreated grey water, and shipping activities.

The entry of North Pacific seawater, containing a relatively high abundance of MPs compared with other global locations (van Sebille et al., 2015; Isobe et al., 2019), may cause MP pollution in this region. The MP concentrations in the Chukchi Sea surface water (0.086–0.31; 0.23 ± 0.07 N m^{-3}) (Mu et al., 2019a) were comparable with those in the Svalbard archipelago south of the Barents Sea (0–1.31; 0.34 ± 0.31 N m^{-3}) (Lusher et al., 2015), when comparing data obtained using similar sampling methods (manta trawling with an ~330 μm mesh). The PET fiber, an exclusive MP component in our Sea ice-I samples, was also the most abundant in the surface water around the Bering Strait (Mu et al., 2019a) and central Arctic (Kanhai et al., 2018), the sea ice of the ACB (Kanhai et al., 2020), and the whales from the Beaufort Sea (Moore et al., 2020), supporting the inflowing Pacific seawater as a strong MP source in the WAO. A small water volume (~0.8 Sv; 1 Sv = 10^6 m^3 s^{-1}), approximately 10 times lower than the Atlantic inflow, enters the WAO through the Bering Strait (Woodgate, 2013). However, in contrast that a substantial amount of the Atlantic inflow immediately returns to the Atlantic, the Pacific water does not return out to the Pacific and circulates around the AB by the clockwise Beaufort Gyre until exiting the Arctic via the Fram Strait and Canadian Archipelago (Woodgate, 2013). The Radon isotope ratios in the surface Beaufort Gyre showed a ~20-year residence time (van der Loeff et al., 1995). Enhanced eddy activity in the Beaufort Gyre due to the decades-long decline in summertime sea ice cover may spin the gyre faster and trap freshwater in its clockwise current, preventing the freshwater from leaving the area (Armitage et al., 2020). Therefore, the MPs delivered by Pacific water may be redistributed and remain in this Beaufort Gyre area longer, causing MP accumulation in the WAO. Numerical simulations have predicted a temporal increase in MP content in North Pacific Ocean water resulting from the continuous plastic debris discharge into the marginal seas of this ocean (Isobe et al., 2019) and the global oceanic circulation concentrating floating plastics in this ocean (van Sebille et al., 2012). In future, the amount of MPs entering the WAO is expected to increase proportionally.

Growing data about air-driven MP in remote regions (Alpine snow (Materić et al., 2020), mountain catchment (Allen et al., 2019), and oceanic air (Liu et al., 2019)) suggest that atmospheric transport and deposition may be another significant MP pathway to the Arctic. We also confirmed the atmospheric long-range transport possibility of MPs from those found in the WAO ice floe snow. However, our results show that the atmospheric input contribution to the MPs entrapped in Arctic sea ice may not be substantial, when based on different MP characteristics and much lower MP load in snow. The estimated snowfall-driven MP flux may be somewhat uncertain since we assumed MPs in snow samples to solely originate from snowfall scavenging. Rainfall, accounting for approximately 60% of precipitation in the Arctic Ocean (Boisvert et al., 2018), can deposit additional MPs. Dry deposition can be also considered to another input path for airborne MP deposits. However, the snowfall-based atmospheric plastic flux estimated here may not change significantly, considering high precipitation frequency (~230 days yr^{-1} for total precipitation event and ~170 days yr^{-1} for snowfall event) in the WAO domain (Boisvert et al., 2018) and fivefold higher scavenging efficiency of a snow flake than a rain droplet (Mackay, 2001). Given that atmospheric transport of MPs into the Arctic is likely enhanced during positive North Atlantic Oscillation phases, particularly in winter and spring (Evangeliou et al., 2020), our Arctic snow measurements collected in summer may underestimate atmospheric input. Arctic river discharge has increased due to global warming (McClelland et al., 2006), which may deliver MPs deposited in the Arctic watershed from the atmosphere into the Arctic Ocean. This additional input was not considered in this basic calculation. To validate our estimation regarding atmospheric fall-out, more measurements reflecting spatio-temporal variation are needed for not only each of MPs deposited via rainfall and snowfall, but also flying MPs in air.

Arctic shipping activities, with fisheries as a major contributor (Eguíluz et al., 2016), could be a local source of Arctic MPs. Our sea ice samples contained various ship paint-based polymers, including varnish, rosin ester, CE-nitrate, and alkyd resin, as well as a fishing gear-associated polymer (e.g., PA). These polymers comprised ~10% of the total MPs in sea ice samples. The more dominant varnish type in the Eurasian sea ice (Peeken et al., 2018) may reflect a geographical difference in shipping activities, which are concentrated in the Norwegian and Barents Seas rather than in the Chukchi and Beaufort Seas (Eguíluz et al., 2016; Cózar et al., 2017). The discharge of land- and ship-based wastewater can be another input source of MPs to the Arctic Ocean, although they are vastly unexplored. Evoked the importance of the land-based Arctic wastewater outlet as a local source of MPs to Svalbard waters. Mikkola (2020) estimated annual load of 10^8–10^9 N $capita^{-1}$ for MP discharge of untreated grey water from cruise ships to the marine environment. Considering the volume of grey water generated by vessels in the Canadian Arctic (~90 kilotons per year) (Vard Marine Inc., 2018), MPs discharged from Arctic shipping fleet to the study domain may not be ignored. A gradual sea ice cover retreat due to global warming, followed by increased shipping activities (Miller and Ruiz, 2014), can gradually increase the contribution of these local sources to the Arctic MP load.

4.3. Possible mechanism for ice-trapped high MPs

Our study confirms the results of the previous studies that sea ice entraps MPs at several orders of magnitude higher than in seawater. Considering the higher abundance of MPs at the air-water interfacial layer (Chae et al. 2015; Anderson et al., 2018) and the drastic decrease in abundances with depth in ocean water (Kooi et al., 2016), it is reasonable to hypothesize that MPs should be preferentially enriched in the uppermost layer of sea ice as seen in fast-packed ice cores under microcosm conditions (Geilfus et al., 2019). However, most of sea ice cores collected in Arctic and Antarctic ice environment exhibited relatively uniform MP abundances throughout the entire ice depth (Peeken et al., 2018; Kanhai et al., 2020; Kelly et al., 2020; this study), indicating that more complicated mechanisms affect MP ice-trapping in real environment. Several plausible mechanisms can be suggested to understand ice-trapped high MPs in the WAO. Analogous to biotic and abiotic particle enrichment in sea ice, MPs can be mechanically concentrated by scavenging of frazil ice crystals rising through the water column and their subsequent coalescence into firm ice layers (Garrison et al., 1989; Nürnberg et al., 1994; Dumont et al., 2009). Brine channels formed in sea ice (Petrich and Eicken, 2010) and coagulation with algae-excreted sticky exopolymers (Long et al., 2015; Galgani et al., 2019) could be another factor driving MP enrichment in sea ice. Considering the abundant formation of ice-algal aggregates below the melting Arctic sea ice (Assmy et al., 2013), the continuing loss of the thick multiyear sea ice layer and its replacement by thin sea ice may

facilitate algae-MP aggregates entrapment in sea ice. Meanwhile, the MPs released together with less dense freshwater (see 0.1–1.1 psu of salinity in MPW) by sea ice melting may mostly remain in the surface/subsurface water in summer due to weakened brine convection and thereafter may be retrapped in the newly formed sea ice in winter. The enriched MP levels (0–18; 5.3 ± 4.4 N m^{-3}) in water beneath ACB sea ice floes (Kanhai et al., 2020) compared with the ice-free surface waters from the Arctic gateway (Lusher et al., 2015; Mu et al., 2019a) supports this hypothesis. Although MPs can eventually settle to the Arctic seafloor, this physical-biological coupling may temporarily impede MP settling and its effect on MP trapping may differently appear at locations along the drift path of a single core. In particular, the WAO experiences the largest summer sea ice loss in the Arctic Ocean (Stroeve and Notz, 2017). The repeated yearly melting and freezing of sea ice may keep MPs in the surface/subsurface water column of this region longer by repeating MP incorporation and release. Thus, sea ice entrapment and amplified gyre-driven circulation, combined with new additions via the Bering Strait, may cause MP accumulation in the WAO. Given the continuing sea ice extent retreat (Stroeve et al., 2012), this combined trapping effect may be enhanced in the future.

4.4. Implication of size distribution

The prevalence of MP at the smallest detectable size class found in previous Arctic samples (Peeken et al., 2018; Bergmann et al., 2019) has created great concerns about the Arctic ecosystem, since smaller MPs can be ingested by organisms in the lower trophic levels of the food web and are able to translocate into the tissues more readily than larger particles (Carbery et al., 2018). The size distributions of MPs in the Eurasian samples (Peeken et al., 2018; Bergmann et al., 2019) were nearly a power-law distribution, which can be predicted by a plastic weathering experiment excluding natural MP removal processes (Song et al., 2017). On the other hand, the WAO samples with Gaussian distributions show that small particles below specific size classes may be more deficient than those observed in Eurasian samples or those expected from a fragmentation model. The Eurasian Arctic samples (Peeken et al., 2018; Bergmann et al., 2019) were analyzed using an imaging FTIR technique to minimize human bias in MP determination, which may influence the different size distributions. However, Gaussian distributions like ours have been frequently observed in open ocean waters, where large particles ≥ 200 to ≥ 500 μm difficult to lose via human error were analyzed (Cózar et al., 2014; Cózar et al., 2017; Serranti et al., 2018; Mu et al., 2019a) and in Antarctic sea ice (Kelly et al., 2020), where the same method (imaging FTIR technique for MPs ≥ 11 μm) used for the Eurasian sea ice and snow samples was applied. Additionally, the fiber MP characteristics found in the WAO samples were consistent with those seen in a global dataset of microfibers collected in oceanic waters with a Gaussian-type size distribution, median size of 1.07 mm, and median thickness of 15.8 μm (Suaria et al., 2020). Because of the abundant surface biofilm/aggregation (Kaiser et al., 2017; Michels et al., 2018) and lower buoyancy velocity (Reisser et al., 2015) caused by high surface area-to-volume ratios, smaller MPs are more susceptible to vertical sinking and wind mixing (Poulain et al., 2019). Thus, small particles are relatively deficient in remote areas compared with coastal areas (Ryan, 2015) and in surface areas compared with submerged water columns (Kooi et al., 2016).

5. Conclusions

To assess the role of WAO as a global sink and an Arctic source of MPs, we investigated the number- and mass-based MP contents separated by size and shape geometry for sea ice, snow, and MPW. The main findings and implications can be summarized as follows.

(1) Our data shows a strong dependency of MP data (concentration, polymer composition, and size distribution) on measured cutoff size and geometry, with dominating numbers of fibers (mostly PET) in large-size classes but nonfibers of other polymers in small-size classes. Thus, the harmonizing the cutoff size and geometry of analyzed MPs is critical to identify linkages among different basins or compartments since MP data alters according to them.

(2) For the same size range and geometry, sea ice MPs in WAO exhibit similar number-based pollution levels with those in EB and ACB but closer similarities in polymer and shape composition to those of ACB. This implies a strong linkage of the two basins (WAO and ACB) by a Transpolar Drift that forms in WAO and thereby a significant role of WAO as Arctic MP source.

(3) Number-based MP concentration tends to increase with decreasing particle size but the opposite trend is found for mass-based values. Consequently, the total MP mass in samples is largely accounted for by large-sized MPs (particularly, nonfibers) rare in numbers. Thus, the presence of large particles, which not only can become source of smaller MPs but are apt to be missed by reducing sample volume, should not be overlooked in plastic mass budgeting.

(4) Snow-captured MPs significantly differed from ice-trapped MPs in concentration, polymer, and size distribution. Estimated MP flux via snowfall accounted for < 1% of ice-trapped MP load in WAO. Despite increasing concern of atmospheric delivery to Arctic, our snow MP data exhibit that atmospheric transport may not be notable pathway to Arctic MPs.

(5) This first mass budget for MPs in Arctic shows that the amount comparable with those afloat at global ocean is trapped in WAO seasonal sea ice. A significant amount of plastic particles, which are lost from the global inventory, may accumulate in the WAO due to temporary sink (sea ice) and oceanic currents (i.e., Bering current and Beaufort Gyre). Our results highlight that the WAO ice zone may be responsible for a sink of global MPs and a source of Arctic MPs.

Supplementary materials

The analysis procedure and QA/QC (section-I), the methods for size distribution of normalized MP concentration (section-II) and MP mass estimation (section-III), air-mass trajectories for 500-m and 1000-m a.s.l. (Fig. S1), vertical profile of MPs in 16SIC core (Fig. S2) and in 17SIC (Fig. S3), size distribution (Fig. S4) and relative contribution in each size class (Fig. S5) of number-based MP concentration, size distribution of mass-based MP concentration (Fig. S6), estimated masses of single MP particle with size (Fig. S7), PCA result comparing nonfiber composition between Eurasian and WAO sea ices (Fig. S8), sampling details for the sea ice, snow, and MPW collected in the WAO (Table S1), and original densities of MP polymer identified by FTIR in this study (Table S2) are provided.

CRediT authorship contribution Statement

Seung-Kyu Kim: Conceptualization, Methodology, Formal analysis, Investigation, Resource, Data curation, Writing - original draft, Writing - review & editing, Visualization, Supervision, Project administration, Funding acquisition. **Hee-Jee Lee:** Formal analysis, Methodology, Validation, Investigation, Data curation, Visualization. **Ji-Su Kim**: Formal analysis, Methodology, Validation, Investigation, Data curation, Visualization. **Sung-Ho Kang:** Conceptualization, Resource, Funding acquisition. **Eun-Jin Yang**: Conceptualization, Resource, Funding acquisition. **Zhexi Tian:** Formal analysis, Visualization. **and Kyoung-Ho Cho**: Formal analysis, Visualization. **Anthony Andrady**: Writing - review & editing.

Declaration of Competing Interest

The authors declare that they have no known competing financial interests or personal relationships that could have appeared to influence the work reported in this paper.

Acknowledgements

This study is the outcome of the IBRV *Araon* R/V expedition. We thank the captain and crew of R/V Araon for their assistance with sample collection. This work was supported by the project titled 'Korea-Arctic Ocean Observing System (K-AOOS), KOPRI, 20160245', funded by the Ministry of Oceans and Fisheries (MOF), Korea. Furthermore, this work was supported by Basic Science Research Program through the National Research Foundation of Korea (NRF) funded by the Ministry of Science and ICT (MSIT) (NRF-2017R1E1A1A01073137) and by R&D Program for Oceans and Polar Regions of the National Research Foundation of Korea (NRF) funded by the Ministry of Science and ICT (MSIT) (NRF-2019M1A5A1101471).

Appendix A. Supporting information

Supplementary data associated with this article can be found in the online version at doi:10.1016/j.jhazmat.2021.125971.

References

Allen, S., Allen, D., Phoenix, V.R., Roux, G.L., Jiménez, P.D., Simonneau, A., Binet, S., Galop, D., 2019. Atmospheric transport and deposition of microplastics in a remote mountain catchment. Nat. Geosci. 12, 339–344. https://doi.org/10.1038/s41561-019-0335-5.

Anderson, Z.T., Cundry, A.B., Croudace, I.W., Warwik, P.E., Celis-Hernandez, O., Stead, J.L., 2018. A rapid method for assessing the accumulation of microplastics in the sea surface microlayer (SML) of estuarine systems. Sci. Rep. 8, 9428. https://doi.org/10.1038/s41598-018-27612-w.

Arctic Sea Ice Monitoring System (ASIMS), 2020. SSMIS sea ice extent. Accessed 30 June 2020. http://seaice.kma.go.kr/arctic/spatialDistribution.monthly.

Armitage, T.W.K., Manucharyan, G.E., Petty, A.A., Kwook, R., Thompson, A.F., 2020. Enhanced eddy activity in the Beaufort Gyre in response to sea ice loss. Nat. Commun. 11, 761. https://doi.org/10.1038/s41467-020-14449-z.

Assmy, P., Ehn, J.K., Fernádez-Méndez, M., Hop, H., Katlein, C., Sundfjord, A., Bluhm, K., Daase, M., Engel, A., Fransson, A., Granskog, M.A., Hudson, S.R., Kristiansen, S., Nicolaus, M., Peeken, I., Enner, A.H.H., Spreen, G., Tatarek, A., Wiktor, J., 2013. Floating ice-algal aggregates below melting Arctic Sea ice. PLOS One 8, 76599. https://doi.org/10.1371/journal.pone.0076599.

Bergmann, M., Műtzel, S., Primke, S., Tekman, M.B., Trachsel, J., Gerdts, G., 2019. White and wonderful? Microplastics prevail in snow from the Alps to the Arctic. Sci. Adv. 5, 1157. https://doi.org/10.1126/sciadv.aax1157.

Boisvert, L.N., Webster, M.A., Petty, A.A., Markus, T., Bromwich, D.H., Cullather, R.I., 2018. Intercomparison of precipitation estimates over the Arctic Ocean and its peripheral seas from reanalyses. J. Clim. 31, 8441–8462. https://doi.org/10.1175/JCLI-D-18-0125.1.

Brandon, J.A., Jones, W., Ohman, M.D., 2019. Multidecadal increase in plastic particles in coastal ocean sediments. Sci. Adv. 5, 0587. https://doi.org/10.1126/sciadv.aax0587.

Brodzik, M.J., Stewart, J.S., 2016. Near-Real-TimeSSM/I-SSMIS EASE-Grid Daily Global Ice Concentration and Snow Extent, Version 5. Boulder, Colorado USA. NASA National Snow and Ice Data Center Distributed Active Archive Center. https://doi.org/10.5067/VF7QO90IHZ99.

Carbery, M., O'Connor, W., Thavamani, P., 2018. Trophic transfer microplastics and mixed contaminants in the marine food web and implications for human health. Environ. Int. 115, 400–409. https://doi.org/10.1016/j.envint.2018.03.007.

Chae, D.–H., Kim, I.–S., Kim, S.–K., Song, Y.K., Shim, W.J., 2015. Abundance and distribution 940 characteristics of microplastics in surface seawaters of the Incheon/Kyeonggi coastal 941 region. Arch. Environ. Contam. Toxicol. 69, 269–278. https://doi.org/10.1007/s00244-015-0173-4.

Comnea-Stancu, I.R., Wieland, K., Ramer, G., Schwaighofer, A., Lendl, B., 2017. On the identification of rayon/viscose as a major fraction of microplastics in the marine environment: discrimination between natural and manmade cellulosic fibers using Frourier Transform Infrared Spectroscopy. Appl. Spectrosc. 71, 939–950. https://doi.org/10.1177/0003702816660725.

Cózar, A., Echevarría, F., González-Gordillo, J.I., Irigoien, X., Úbeda, B., Hernández-León, S., Palma, Á.T., Navarro, S., García-de-Lomas, J., Ruiz, A., Fernández-de-Puelles, M.L., Duarte, C.M., 2014. Plastic debris in the open ocean. PNAS 111, 10239–10244. https://doi.org/10.1073/pnas.1314705111.

Cózar, A., Marti, E., Duarte, C.M., Garcia-de-Lomas, J., van Sebille, E., Balatore, T.J., Eguiluz, V.C.M., González-Gordillo, I., Perotti, M.L., Echevarria, F., Troublè, R., Irigoien, X., 2017. The Arctic Ocean as a dead end for floating plastics in the North Atlantic branch of the thermohaline circulation. Sci. Adv. 3, 1600582 https://doi.org/10.1126/sciadv.1600582.

Draxler, R., Rolph, G., 2003. HYSPLIT (HYbridSingle-Particle Lagrangian Integrated Trajectory) Model Access via NOAA ARLREADY Website. http://www.arl.noaa.gov/ready/hysplit4.Html. NOAA AirResources Laboratory, Silver Spring: MD.

Dumont, I., Schoemann, V., Lannuzel, D.L., Chou, L., Tison, J.–L., Beequevort, S., 2009. Distribution and characterization of dissolved and particulate organic matter in Antarctic pack ice. Polar Biol. 32, 733–750. https://doi.org/10.1007/s00300-008-0577-y.

Eguíluz, V.M., Fernández-Gracia, J., Irigoien, X., Duarte, C.M., 2016. A quantitative assessment of Arctic shipping in 2010-2014. Sci. Rep. 6, 30682. https://doi.org/10.1038/srep30682.

Eriksen, M., Lebreton, L.C.M., Carson, H.S., Thiel, M., Moore, C.J., Borerro, J.C., Galgani, F., Ryan, P.G., Reisser, J., 2014. Plastic pollution in the world's oceans: more than 5 trillion plastic pieces weighing over 250,000 tons afloat at sea. PLoS ONE 9, 111913. https://doi.org/10.1371/journal.pone.0111913.

Evangeliou, N., Grythe, H., Klimont, Z., Heyes, C., Eckhardt, S., Lopez-Aparicio, S., Stohl, A., 2020. Atmospheric transport is a major pathway of microplastics to remote regions. Nat. Commun. 11, 3381. https://doi.org/10.1038/s41467-020-17201-9.

Fisher, M., Scholz-Böttcher, B.M., 2017. Simultaneous trace identification and quantification of common types of microplastics in environmental samples by pyrolysis-gas chromatography-mass spectrometry. Environ. Sci. Technol. 51, 5052–5060. https://doi.org/10.1021/acs.est.6b06362.

Galgani, L., Tsapakis, M., Pitta, P., Tsiola, A., Tzempelikou, E., Kalantzi, I., Esposito, C., Loiselle, A., Tsotskou, A., Zivanovic, S., 2019. Microplastics increase the marine production of particulate forms of organic matter. Environ. Res. Lett. 14, 124085 https://doi.org/10.1088/1748-9326/ab59ca.

Garrison, D.L., Close, A.R., Reimnitz, E., 1989. Algae concentrated by frazil ice: evidence from laboratory experiments and field measurements. Antarct. Sci. 1, 313–316. https://doi.org/10.1017/S0954102089000477.

Geilfus, N.-X., Munson, K.M., Sousa, J., Germanov, Y., Bhugaloo, S., Babb, D., Wang, F., 2019. Distribution and impacts of micropalstic incorporation within sea ice. Mar. Pollut. Bull. 145, 463–473. https://doi.org/10.1016/j.marpolbul.2019.06.029.

Geyer, R., Jambeck, J.R., Law, K.L., 2017. Production, use, and fate of all plastics ever made. Sci. Adv. 3, e1700782 https://doi.org/10.1126/sciadv.1700782.

Hidalgo-Ruz, V., Gutow, L., Thompson, R.C., Thiel, M., 2012. Microplastics in the marine environment: a review of the methods used for identification and quantification. Environ. Sci. Technol. 46, 3060–3075. https://doi.org/10.1021/es2031505.

Isobe, A., Iwasaki, S., Uchida, K., Tokai, T., 2019. Abundance of non-conservative microplastics in the upper ocean from 1957 to 2066. Nat. Commun. 10, 417. https://doi.org/10.1038/s41467-019-08316-9.

Jambeck, J.R., Geyer, R., Wilcox, C., Siegler, T.R., Perryman, M., Andrady, A., Narayan, R., Law, K.L., 2015. Plastic waste inputs from land into the ocean. Science 347, 768–771. https://doi.org/10.1126/science.1260352.

Kaiser, D., Kowalski, N., Waniek, J.J., 2017. Effects of biofouling on the sinking behavior of microplastics. Environ. Res. Lett. 12, 124003 https://doi.org/10.1088/1748-9326/aa8e8b.

Kanhai, L.D.K., Gardfeldt, K., Lyashevska, O., Hassellov, M., Thompson, R.C., O'Connor, I., 2018. Microplastics in sub-surface waters of the Arctic Central Basin. Mar. Pollut. Bull. 8–18. https://doi.org/10.1016/j.marpolbul.2018.03.011.

Kanhai, L.D.K., Gardfeldt, K., Krumpen, T., Thompson, R., O'Connor, I., 2020. Microplastics in sea ice and seawater beneath ice floes from the Arctic Ocean. Sci. Rep. 10, 5004. https://doi.org/10.1038/s41598-020-61948-6.

Kelly, A., Lannuzel, D., Rodemann, T., Meiners, K.M., Auman, H.J., 2020. Microplastic contamination in east Antarctic sea ice. Mar. Pollut. Bull. 154, 111130 https://doi.org/10.1016/j.marpolbul.2020.111130.

Kim, J.–S., Lee, H.–J., Kim, S.–K., Kim, H.–J., 2018. Global pattern of microplastics (MPs) in commercial food-grade salts: sea salt as an indicator of seawater MP pollution. Environ. Sci. Technol. 52, 12819–12828. https://doi.org/10.1021/acs.est.8b04180.

Kim, S.-K., Song, N.-S., 2021. Microplastics in edible salt: a literature review focusing on uncertainty related with measured minimum cutoff sizes. Curr. Opin. Food Sci. 41, 16–25. https://doi.org/10.1016/j.cofs.2021.02.010.

Kim, S.-K., Kim, J.-S., Lee, H., Lee, H.-J., 2021. Abundance and characteristics of microplastics in soils with different agricultural practices: importance of sources with internal origin and environmental fate. J. Hazard. Mater. 403, 123997 https://doi.org/10.1016/j.jhazmat.2020.123997.

Kooi, M., Koelmans, A.A., 2019. Simplifying microplastic via continuous probability distributions for size, shape, and density. Environ. Sci. Technol. 6, 551–557. https://doi.org/10.1021/acs.estlett.9b00379.

Kooi, M., Reisser, J., Slat, B., Ferrari, F.F., Schmid, M.S., Cunsolo, S., Brambini, R., Noble, K., Sirks, L.–A., Linders, T.E.W., Schoeneich-Argent, R.I., Koelmans, A.A., 2016. The effect of particle properties on the depth profile of buoyant plastics in the ocean. Sci. Rep. 6, 33882. https://doi.org/10.1038/srep33882.

Kűhn, S., Schaafsma, F., van Werven, B., Flores, H., Bergmann, M., Egelkraut-Hotus, M., Tekman, M.B., van Franeker, J.A., 2018. Plastic ingestion by juvenile polar cod (Boreogadus saida) in the Arctic Ocean. Polar Biol. 41, 1269–1278. https://doi.org/10.1007/s00300-018-2283-8.

Law, K.L., Morét-Ferguson, S.E., Goodwin, D.S., Zettler, E.R., DeForce, E., Kukulka, T., Proskurowski, G., 2014. Distribution of surface plastic debris in the eastern Pacific Ocean from an 11-year data set. Environ. Sci. Technol. 48, 4732–4738. https://doi.org/10.1021/es4053076.

Lebreton, L.C.M., van der Zwet, J., Damsteeg, J.W., Slat, B., Andrady, A., Reisser, J., 2017. River plastic emissions to the world's oceans. Nat. Commun. 8, 15611. https://doi.org/10.1038/ncomms15611.

Lee, H.-J., Song, N.-S., Kim, J.-S., Kim, S.-K., 2021. Variation and uncertainty of microplastics in commercial table salts: critical review and validation. J. Hazard. Mater. 402, 123743 https://doi.org/10.1016/j.jhazmat.2020.123743.

Liu, K., Wu, T., Wang, X., Song, Z., Zong, C., Wei, N., Li, D., 2019. Consistent transport of terrestrial microplastics to the ocean through atmosphere. Environ. Sci. Technol. 53, 16012–16019. https://doi.org/10.1021/acs.est.9b03427.

Long, M., Moriceau, B., Gallinari, M., Lambert, C., Huvet, A., Raffray, J., Soudant, P., 2015. Interactions between microplastics and phytoplankton aggregates: impact on their respective fates. Mar. Chem. 175, 39–46. https://doi.org/10.1016/j.marchem.2015.04.003.

Lusher, A.L., Tirelli, V., O'Connor, I., Officer, R., 2015. Microplastics in Arctic polar waters: the first reported values of particles in surface and sub-surface samples. Sci. Rep. 5, 14947. https://doi.org/10.1038/srep14947.

Mackay, D., 2001. Multimedia Environmental Models-The Fugacity Approach. CRC Press, Boca Raton.

Materić, D., Kasper-Giebl, A., Kau, D., Anten, M., Greilinger, M., Ludewig, E., van Sebille, E., Röckmann, T., Holzinger, R., 2020. Micro- and nanoplastics in Alpine snow: a new method for chemical identification and (semi)quantification in the nanogram range. Environ. Sci. Technol. 54, 2353–2359. https://doi.org/10.1021/acs.est.9b07540.

McClelland, J.W., Dery, S.J., Peterson, B.J., Holmes, R.M., Wood, E.F., 2006. A pan-Arctic evaluation of changes in river discharge during the latter half of the 20th century. Geophys. Res. Lett. 33, L06715 doi:06710.01029/02006GL025753.

Michels, J., Stippkugel, A., Lenz, M., Wirtz, K., Engel, A., 2018. Rapid aggregation of biofilm-covered microplastics with marine biogenic particles. Proc. Biol. Sci. 285, 1885. https://doi.org/10.1098/rspb.2018.1203.

Mikkola, O., 2020. Estimating Microplastic Concentrations and Loads in Cruise Ship Grey Waters. Thesis for the degree of Master, Aalto University.

Miller, A.W., Ruiz, G.M., 2014. Arctic shipping and marine invaders. Nat. Clim. Change 4, 413–416. https://doi.org/10.1038/nclimate2244.

Moore, R.C., Loseto, L., Noel, M., Etemadifar, A., Brewster, J.D., MacPhee, S., Bendell, L., Ross, P.S., 2020. Microplastics in beluga whales (Delphinapterus leucas) from the eastern Beaufort Sea. Mar. Pollut. Bull. 150, 110723 https://doi.org/10.1016/j.marpolbul.2019.110723.

Mu, J., Zhang, S., Qu, L., Jin, F., Fang, C., Ma, X., Zhang, W., Wang, J., 2019a. Microplastics abundance and characteristics in surface waters from the Northwest Pacific, the Bering Sea, and the Chukchi Sea. Mar. Pollut. Bull. 143, 58–65. https://doi.org/10.1016/j.marpolbul.2019.04.023.

Mu, J., Qu, L., Jin, F., Zhang, S., Fang, C., Ma, X., Zhang, W., Huo, C., Cong, Y., Wang, J., 2019b. Abundance and distribution of microplastics in the surface sediments from the northern Bering and Chukchi Seas. Environ. Pollut. 245, 122–130. https://doi.org/10.1016/j.envpol.2018.10.097.

Nicolaus, M., Katlein, C., Maslanik, J., Hendricks, S., 2012. Changes in Arctic sea ice result in increasing light transmittance and absorption. Geophys. Res. Lett. 39, 2012GL053738 https://doi.org/10.1029/2012GL053738.

Nolin, A.W., Armstrong, R., Maslanik, J., 1998. Near-Real-Time SSM/I-SSMIS EASE-Grid Daily Global Ice Concentration and Snow Extent, Version 4. Boulder, Colorado USA. NASA National Snow and Ice Data Center Distributed Active Archive Center. https://doi.org/10.5067/VF7QO90IHZ99.

Nürnberg, D., Wollenburg, I., Dethleff, D., Eicken, H., Kassens, H., Letzig, T., Reimnitz, E., Thiede, J., 1994. Sediments in Arctic sea ice-implications for entrainment. Transp. Release Mar. Geol. 119, 185–214. https://doi.org/10.1016/0025-3227(94)90181-3.

Obbard, R.W., Sadri, S., Wong, Y.Q., Khitun, A.A., Baker, I., Thompson, R.C., 2014. Global warming releases microplastic legacy frozen in Arctic sea ice. Earth's Future 2, 315–320. https://doi.org/10.1002/2014EF000240.

Peeken, I., Primpke, S., Beyer, B., Gütermann, J., Katlein, C., Krumpen, T., Bergmann, M., Hehemann, L., Gerdts, G., 2018. Arctic sea ice is an important temporal sink and means of transport for microplastic. Nat. Commun. 9, 1505. https://doi.org/10.1038/s41467-018-03825-5.

Petrich, C., Eicken, H., 2010. Growth, structure and properties of sea ice. In: Thomas, D. N., Dieckmann, G.S. (Eds.), Sea Ice, third edition. Blackwell Publishing Ltd, Oxford, pp. 23–77. https://doi.org/10.1002/9781444317145.

Petty, A.A., Hutchings, J.K., Richter-Menge, J.A., Tschudi, M.A., 2016. Sea ice circulation around the Beaufort Gyre: the changing role of wind forcing and the sea ice state. J. Geophys. Res. Oceans 121, 3278–3296. https://doi.org/10.1002/2015JC010903.

Poulain, M., Mercier, M.J., Brach, L., Martignac, M., Routaboul, C., Perez, E., Desjean, M. C., Halle, A., 2019. Small microplastics as a main contributor to plastic mass balance in the North Atlantic subtropical gyre. Environ. Sci. Technol. 53, 1157–1164. https://doi.org/10.1021/acs.est.8b05458.

Reisser, J., Slat, B., Noble, K., Plessis, K., Epp, M., Proietti, M., Sonneville, J., Becker, T., Pattiaratchi, C., 2015. The vertical distribution of buoyant plastics at sea: an observational study in the North Atlantic Gyre. Biogeosciences 12, 1249–1256. https://doi.org/10.5194/bg-12-1249-2015.

Renner, A.H.H., Gerland, S., Haas, C., Spreen, G., Beckers, J.F., Hansen, E., Nicolaus, M., Goodwin, H., 2014. Evidence of Arctic sea ice thinning from direct observations. Geophys. Res. Lett. 41, 5029–5036. https://doi.org/10.1002/2014GL060369.

Ryan, P.G., 2015. Does size and buoyancy affect the long-distance transport of floating debris? Environ. Res. Lett. 10, 084019 https://doi.org/10.1088/1748-9326/10/8/084019.

Serranti, S., Palmieri, R., Bonifazi, G., Cózar, A., 2018. Characterization of microplastic litter from oceans by an innovative approach based on hyperspectral imaging. Waste Manag. 76, 117–125. https://doi.org/10.1016/j.wasman.2018.03.003.

Song, Y.K., Hong, S.H., Jang, M., Han, G.M., Jung, S.W., Shim, W.J., 2017. Combined effects of UV exposure duration and mechanical abrasion on microplastic fragmentation by polymer type. Environ. Sci. Technol. 51, 4368–4376. https://doi.org/10.1021/acs.est.6b06155.

Sørensen, L., Groven, A.S., Hovsbakken, I.A., Puerto, O.D., Krause, D.F., Sarno, A., Booth, A.M., 2021. UV degradation of natural and synthetic microfibers causes fragmentation and release of polymer degradation products and chemical additives. Sci. Total Environ. 755, 143170 https://doi.org/10.1016/j.scitotenv.2020.143170.

Spreen, G., Kaleschke, L., Heygster, G., 2008. Sea ice remote sensing using AMSR-E 89 GHz channels. J. Geophys. Res. 113, C02S03. https://doi.org/10.1029/2005JC003384.

Stroeve, J., Notz, D., 2018. Changing state of Arctic sea ice across all seasons. Environ. Res. Lett. 13, 103001 https://doi.org/10.1088/1748-9326/aade56.

Stroeve, J.C., Serreze, M.C., Holland, M.M., Kay, J.E., Malanik, J., Barrett, A.P., 2012. The Arctic's rapidly shrinking sea ice cover: a research synthesis. Clim. Chang. 110, 1005–1027. https://doi.org/10.1007/s10584-011-0101-1.

Suaria, G., Achtypi, A., Perold, V., Lee, J.R., Pierucci, A., Bornman, T.G., Aliani, S., Ryan, P.G., 2020. Microfibers in oceanic surface waters: a global characterization. Sci. Adv. 6, 8493. https://doi.org/10.1126/sciadv.aay8493.

Tekman, M.B., Krumpen, T., Bergmann, M., 2017. Marine litter on deep Arctic seafloor continues to increase and spreads to the North at the HAUSGARTEN observatory. Deep Sea Res. Part I Ocean. Res. Pap. 120, 88–99. https://doi.org/10.1016/j.dsr.2016.12.011.

Timco, G.W., Frederking, R.M.W., 1996. A review of sea ice density. Cold Reg. Sci. Technol. 24, 1–6. https://doi.org/10.1016/0165-232X(95)00007-X.

Tschudi, M., Meier, W.N., Stewart, J.S., Fowler, C., Maslanik, J., 2019. Polar Pathfinder Daily 25 km EASE-Grid Sea Ice MotionVectors, Version 4. Boulder, Colorado USA. NASA National Snow and Ice DataCenter Distributed Active Archive Center. https://doi.org/10.5067/INAWUWO7QH7B.

van der Loeff, M.M.R., Key, R.M., Scholten, J., Bauch, D., Michel, A., 1995. 228Ra as a tracer for shelf water in the Arctic Ocean. Deep-Sea Res. II 42, 1533–1553. https://doi.org/10.1016/0967-0645(95)00053-4.

van Sebille, E., England, M.H., Froyland, G., 2012. Origin, dynamics and evolution of ocean garbage patches from observed surface drifters. Environ. Res. Lett. 7, 044040 https://doi.org/10.1088/1748-9326/7/4/044040.

van Sebille, E., Wilcox, C., Lebreton, L., Maximenko, N., Hardesty, B.D., van Franeker, J. A., Eriksen, M., Siegel, D., Galgani, F., Law, K.L., 2015. A global inventory of small floating plastic debris. Environ. Res. Lett. 10, 124006 https://doi.org/10.1088/1748-9326/10/12/124006.

Vard Marine Inc, 2018. Canadian Arctic greywater report: estiamtes, forecasts, and treatment technologies. Report #360-000, Rev 2. Accessed 30 March 2021.

Warren, S.G., Rigor, I.G., Untersteiner, N., 1999. Snow depth on Arctic sea ice. J. Clim. 12, 1814–1829. https://doi.org/10.1175/1520-0442(1999)012<1814:SDOASI>2.0.CO;2.

Woodgate, R., 2013. Arctic ocean circulation: going around at the top of the world. Nat. Educ. Knowl. 4, 8. https://www.nature.com/scitable/knowledge/library/arctic-ocean-circulation-going-around-at-the-102811553/.